metals

MDPI

Article

Micro-Tensile Characterization of Heterogeneous Girth Welds in Unequal Wall Thickness X80/X60 Pipelines

Ke Wang [1,2], Min Zhang [1,*], Junfeng Cao [3], Chaocheng Tan [4], Jihong Li [1], Weifeng Ma [2], Hailiang Nie [2] and Junjie Ren [2]

[1] Faculty of Materials Science and Engineering, Xi'an University of Technology, Xi'an 710048, China
[2] Tubular Goods Research Institute, China National Petroleum Corporation (CNPC), Xi'an 710077, China
[3] Production and Operation Department, Changqing Oilfield Company, Xi'an 710018, China
[4] The Tenth Oil Production Plant, Changqing Oilfield Company, Qingyang 745199, China
* Correspondence: zhmmn@xaut.edu.cn

Abstract

The structural integrity of pipeline girth welds is critical, especially when the welds involve heterogeneous materials and non-uniform wall thicknesses. Current evaluation methods that compare the strength of the weld to that of the base metal (BM) are inadequate for such complex welds. This paper addresses this gap by applying micro-tensile specimen testing to characteristic zones within heterogeneous girth welds that exhibit non-uniform wall thicknesses. We conducted tensile performance tests on X80 and X60 steel pipes featuring unequal wall thickness butt joints. The analysis focused on the wall thickness direction of the girth weld as well as the transverse direction, examining differences and patterns in performance across various regions. The findings provide an improved understanding of property gradients in heterogeneous girth welds and offer practical guidance for more reliable safety evaluation of pipelines with unequal wall thickness joints.

Keywords: girth welds; mechanical properties; heterogeneous; non-uniform wall thickness; characteristic zones

1. Introduction

As a relatively weak component of long-distance pipeline systems, the safety of girth welds directly impacts the overall reliability of the pipeline [1–5]. This issue becomes particularly complex when dealing with girth welds that involve heterogeneous materials and non-uniform wall thicknesses. Currently, the most prevalent safety evaluation method for girth welds internationally involves comparing the tensile strength of the weld material with that of the base material [6–8]. However, this method is inadequate for evaluating heterogeneous girth welds with non-uniform wall thicknesses. Consequently, there is an urgent need to conduct in-depth studies on the tensile properties of these types of girth weld joints to identify their differences [9–11].

Accurate testing and characterization of the mechanical properties of girth welds provide the foundation for determining region-specific material properties and for subsequent safety evaluation [12–14]. Numerous studies have attempted to investigate the constitutive behavior of girth welds using various methods [15–18]. For example, Adeeb et al. [19] conducted tensile tests on a specific X100 pipe girth weld joint specimen using Digital Image Correlation (DIC) technology. They observed that the strength of the weld metal (WM) surpassed that of the base material, which was attributed to strain concentration resulting from the softening of the heat-affected zone (HAZ). Similarly, Wu et al. [20] employed DIC

Check for updates

Academic Editor: Masahiro Fukumoto

Received: 20 January 2026
Revised: 13 February 2026
Accepted: 22 February 2026
Published: 26 February 2026

Copyright: © 2026 by the authors. Licensee MDPI, Basel, Switzerland. This article is an open access article distributed under the terms and conditions of the Creative Commons Attribution (CC BY) license.

technology to assess the local tensile properties of an X80 pipe girth weld joint specimen, revealing that the yield strength of the HAZ and WM at the joint was inferior to that of the BM. Furthermore, Cao et al. [21] examined the strain limits of materials in various regions of an X70 pipe girth weld joint under different stress states, noting that the strength of the WM and HAZ at the joint was lower than that of the BM, with the WM demonstrating the lowest strain limit under tensile loading. Collectively, these studies highlight that girth welds are heterogeneous materials, often juxtaposed with homogeneous materials on both sides, thus complicating the performance of heterogeneous non-uniform wall thickness girth welds.

Due to the influence of welding rod materials, welding methods, and the structures on both sides of the girth weld, the mechanical properties of the weld exhibit significant variations in different regions [5,9,22]. Because the range of each region is relatively small, sample preparation is very challenging. Testing the micro-region tensile mechanical properties of girth welds has become a major challenge in practical engineering. Tang et al. [23], Zhu [24], and Nie et al. [25] proposed a method based on the natural morphology of the weld structure to perform characteristic partitioning, followed by slow wire cutting of micro-region tensile specimens from each area, and then conducting performance tests. This method has currently been validated for homogeneous, uniform-thickness girth weld joints, but no related research has been conducted on heterogeneous, non-uniform wall thickness girth welds.

This paper investigates girth welds in heterogeneous pipes with non-uniform wall thickness. A micro-tensile specimen approach is adopted to perform mechanical tests on various characteristic zones across the girth weld cross-section. The spatial distribution of material properties in these zones is examined, and the underlying causes of the observed variations are analyzed. The results provide valuable guidance for the safety evaluation of heterogeneous girth welds in unequal wall thickness pipelines.

2. Materials and Experimental Methods

2.1. Materials

The girth welds of pipelines at a station of the West–East Gas Pipeline Phase III are butt-welded using X80 and X60, with a V-groove preparation. The X80 pipeline has a specification of Φ914 mm × 33 mm, while the X60 pipeline has a specification of Φ914 mm × 22 mm. The chemical compositions of X80 base metal, X60 base metal and girth weld joints are shown in Table 1.

Table 1. Chemical composition of base metal and girth weld (wt.%).

Materials	C	Mn	Si	Ni	Mo	Fe
X80 Base metal	0.070	1.68	0.19	0.21	0.20	Bal.
X60 Base metal	0.059	1.36	0.21	0.011	0.03	Bal.
Girth weld	0.068	1.69	0.20	0.21	0.20	Bal.

2.2. Welding Process

This test is conducted in accordance with Q/SY GJX0221-2012 "Technical Specification for Welding of Station Pipeline Networks in the West–East Gas Pipeline Phase III Project" [26]. The specific welding process is Gas Tungsten Arc Welding + Shielded Metal Arc Welding (GTAW + SMAW). Manual root welding is performed using ER50-6 model Φ2.5 mm welding wire by Atlantic China Welding Consumables, Inc., Zigong, China, with reference to the standard GB/T8110-2008 "Welding electrodes and rods for gas shielding arc welding of carbon and low alloy steel" [27]. Manual filling welding is conducted using E6015-G model Φ3.2 mm electrodes by Atlantic China Welding Consumables, Inc.,

Zigong, China, and manual capping welding is performed with Φ3.2 mm electrodes, both complying with the standard GB/T5118-2012 "Covered electrodes for manual metal arc welding of creep-resisting steels" [28]. The cross-section of the girth weld consists of 1 root weld layer, 2–8 filling weld layers, and 1 capping weld layer. Parallel welding is permitted for filling and capping layers, with 2–4 layers welded side by side per layer. The welding butt joint adopts external surface alignment, with the root section of unequal wall thickness being beveled at a 20° angle.

2.3. Micro-Zone Division

According to the welding structure, the welding structure is divided into different areas. Figure 1 shows a typical sweat microstructure. The base metal zone of X80 steel consists of granular bainite, while that of X60 steel is primarily granular bainite with polygonal ferrite and a small amount of pearlite. The root weld at the center of the weld is composed of granular bainite and polygonal ferrite, whereas the fill weld and cap weld are mainly acicular ferrite, containing granular bainite and polygonal ferrite. The coarse-grained heat-affected zone (HAZ) on the X80 steel side is granular bainite, while the fine-grained HAZ on the X80 steel side is predominantly polygonal ferrite, containing a mixture of martensite, retained austenite, and granular bainite. The coarse-grained HAZ on the X60 steel side is mainly granular bainite with polygonal ferrite and pearlite, and the fine-grained HAZ on the X60 steel side is primarily polygonal ferrite, containing a mixture of martensite, retained austenite, and pearlite. As shown, many welded areas have micromorphic forms and particles of different sizes, which can be effectively distinguished into individual areas. The welded structures include a cap weld, filling weld, root bead, HAZ, X60 steel BM and X80 steel base metal.

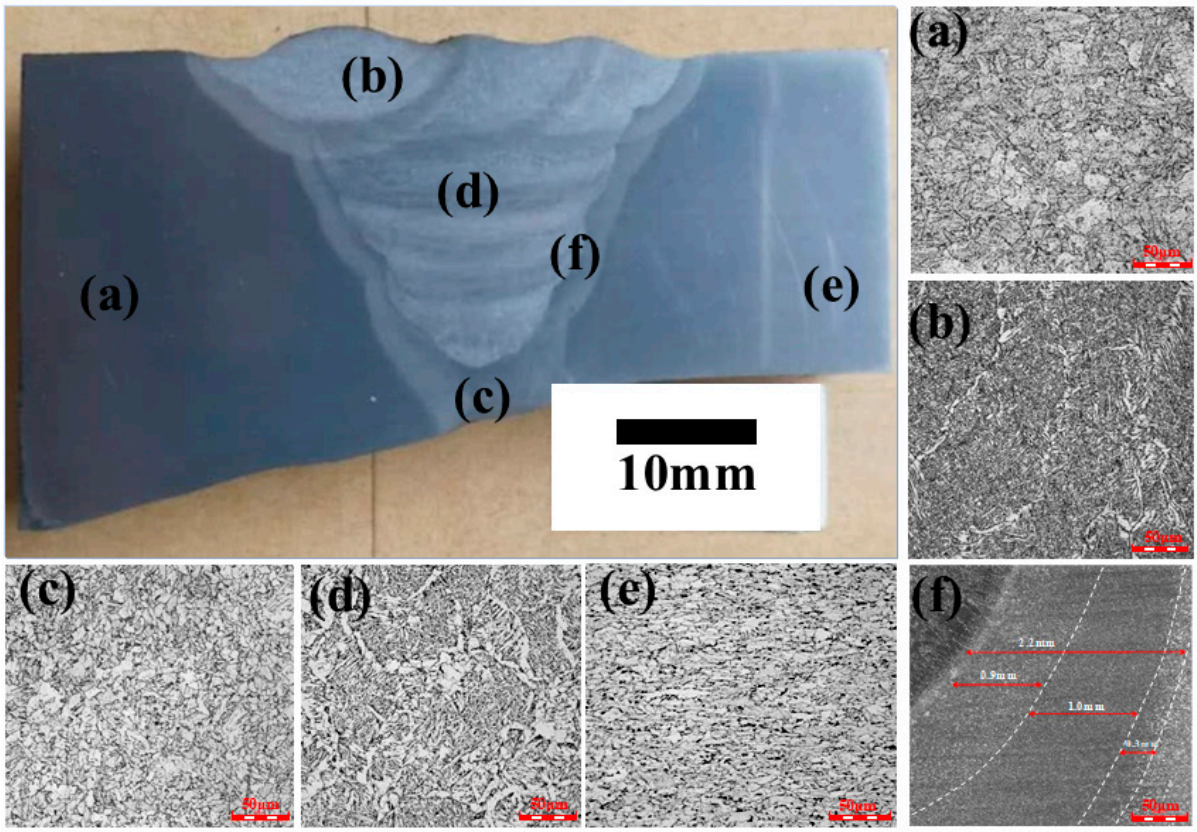


Figure 1. Representative image of the sample and SEM images taken from different regions ((**a**). X80 steel base metal, (**b**). gap weld, (**c**). root bead, (**d**). filling weld, (**e**). X60 steel base metal, (**f**). heat-affected zone).

The various regions of the girth weld structure are categorized and numbered as depicted in Figure 2. In this figure, the segments labeled a11–a54 correspond to the capping zone, while bs11–bs53, bz11–bz42, and bx1–bx4 denote the filling zone. The root zone is represented by c1–c2, and the heat-affected zone is indicated by d1–d4 and ne1–ne4. Additionally, the X80 series and X60 series refer to the base metal zone.

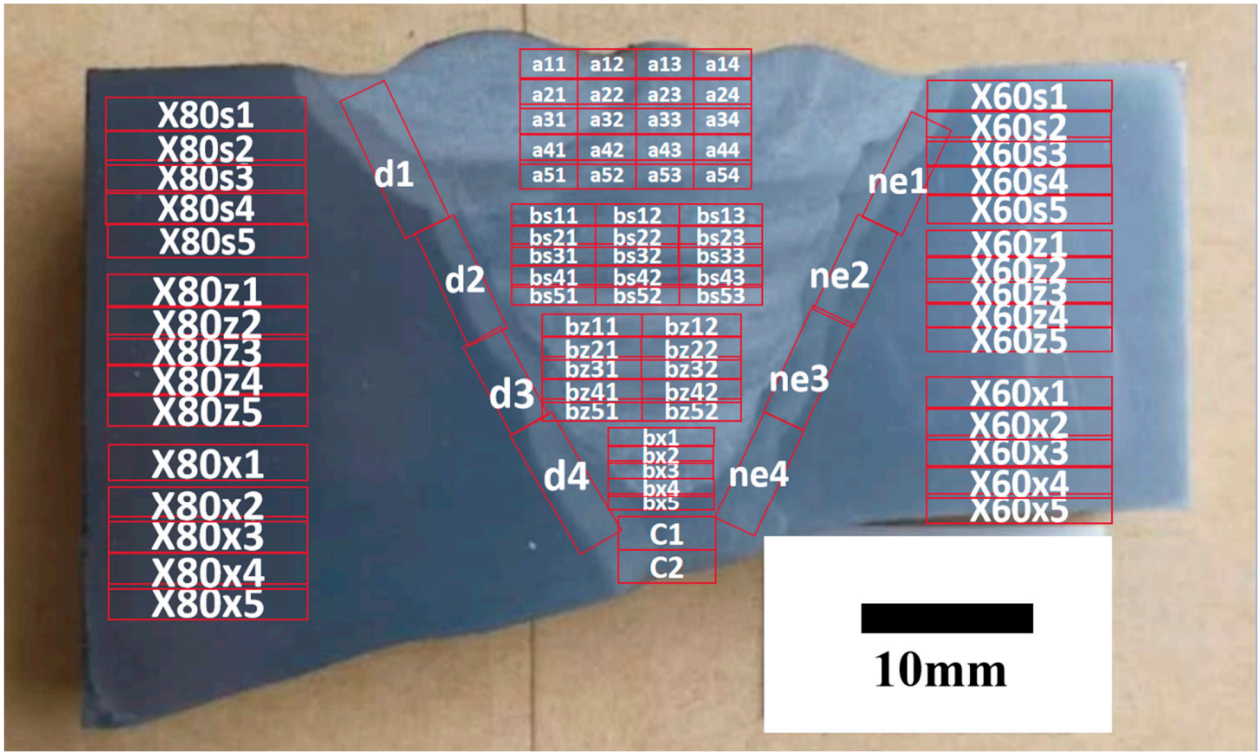


Figure 2. Photograph showing the characteristic zones and specimen distribution design.

The specimen processing method is illustrated in Figure 3. The selected machining section was cut perpendicularly to the weld direction, resulting in a billet that is longer than the specimen itself. Both cutting surfaces of the billet were polished to ensure they were smooth and parallel. The cap weld, filling weld, root bead, and heat-affected zones of the weld were revealed by applying a weld corrosion solution to one end face of the billet.

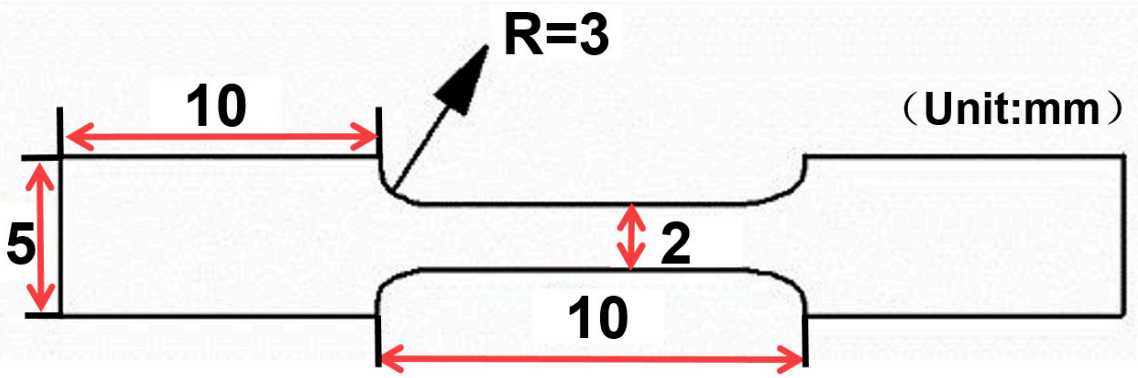


Figure 3. Schematic of specimen geometry (thickness: 0.8 mm).

2.4. Sample Processing

The micro-tensile specimens were prepared using a slow wire cutting technique, with the tensile direction aligned along the circumferential direction of the girth weld

structure, which is perpendicular to the plane depicted in Figure 2 and oriented inward. Figure 3 illustrates the schematic diagram of the specimen's shape and dimensions, with the specimen thickness measuring approximately 0.8 mm.

Each processed specimen is initially ground with 400-grit sandpaper to eliminate surface wire cutting marks and stains. This is followed by polishing using 1500-grit sandpaper, after which the specimens are thoroughly cleaned. Prior to testing each specimen, the dimensions of the gauge section are measured, with each parameter assessed three times to obtain an average value.

2.5. Experimental Testing

Quasi-static experiments were conducted using the Instron 5848 quasi-static testing equipment produced by Instron Corporation (Norwood, MA, USA) at a strain rate of 5×10^{-4}. The experimental setup is illustrated in Figure 4. Load data during the experiments were obtained from the 2000 N load cell of the testing apparatus. Strain measurements were acquired using a video extensometer integrated with the testing equipment, which monitored two manually marked white dots on the gauge section of the specimen. The video extensometer was calibrated prior to the experiments to ensure accuracy and reliability. The manually marked white dots are depicted in Figure 5. Before clamping each specimen, the load was zeroed, and then the specimen was mounted. After mounting, the preload was adjusted to within 10 N by fine-tuning the displacement, after which the test commenced. This procedure was repeated for each experiment. Photographs of the specimen were taken before each experiment and after its completion, with each set of data named and numbered according to the designated zones.



Figure 4. Instron 5848 quasi-static testing equipment based on video extensometer.

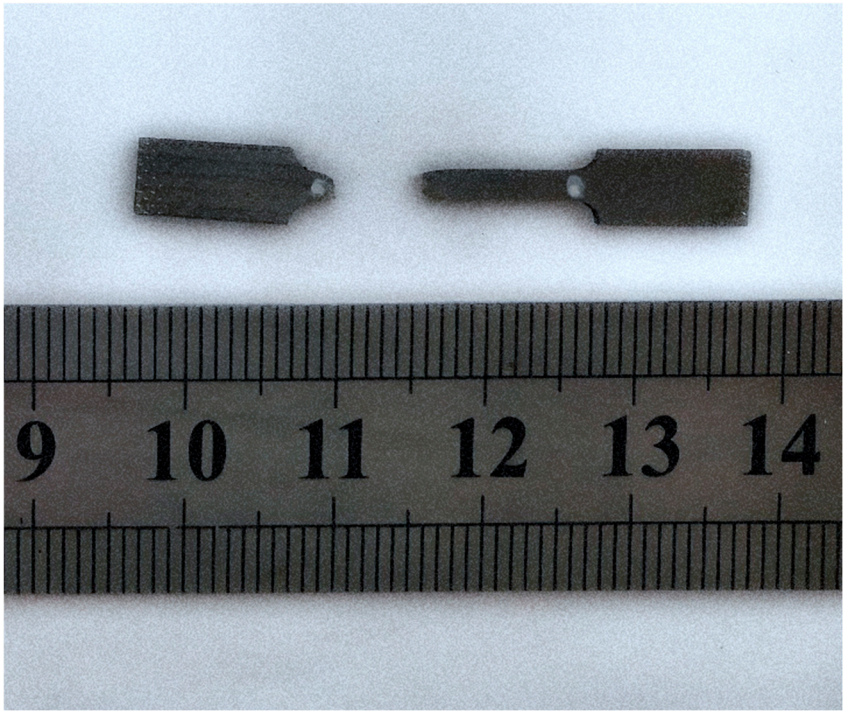


Figure 5. Specimen diagram with white markings indicating video extensometers.

3. Results and Discussion

3.1. Weld Area

The uniaxial tensile test results of specimens from the cap weld are shown in Figure 6a–e. At four transverse positions along the cap weld, five specimens were tested at each position, with a11–a51 located near the HAZ on the X80 steel side and a14–a54 near the HAZ on the X60 steel side. The data exhibits a notable degree of dispersion. Notably, the data in position a12–a52 demonstrates good overlap. Additionally, the yield strength and tensile strength of the cap weld zone show variability across different subzones. In comparison, positions a11–a51 and a14–a54, which are closer to the heat-affected zone, exhibit higher yield strength than positions a12–a52 and a13–a53. Furthermore, the tensile strength displays a gradual decreasing trend from the X80 side to the X60 side.

Figures 7–9 present the results of uniaxial tensile tests on the filling weld specimens. In Figure 7, the specimen is taken from the upper part of the filling weld, close to the cap weld area. Figure 8 shows the specimen from the middle section of the filling weld, while Figure 9 illustrates the specimen from the lower part of the filling weld, near the root bead.

Three transverse positions along the upper filling weld were tested, with five specimens at each position. The specimens bs11–bs51 were located near the heat-affected zone of X80 steel, while bs13–a53 were near the heat-affected zone of X60 steel. The experimental data exhibited significant dispersion characteristics. In contrast, the yield strength of specimens bs12–bs52 was the highest, surpassing that of specimens bs11–bs51 and bs13–a53. The tensile strength showed a gradual decreasing trend from the X80 side to the X60 side.

Two transverse positions along the middle filling weld were tested, with five specimens at each position. Notably, specimens bz51 and bz52 experienced failure during testing, resulting in the absence of valid data. The specimens bz11–bz51 were located near the heat-affected zone of the X80 steel, while bz12–bz52 were situated near the heat-affected zone of the X60 steel. The yield strength of bz11–bz51 was 553 MPa, with a tensile strength of 690 MPa, while the yield strength of bz11–bz51 was 522 MPa, with a tensile strength of 681 MPa. There is a gradual decrease in strength from the X80 side to the X60 side.

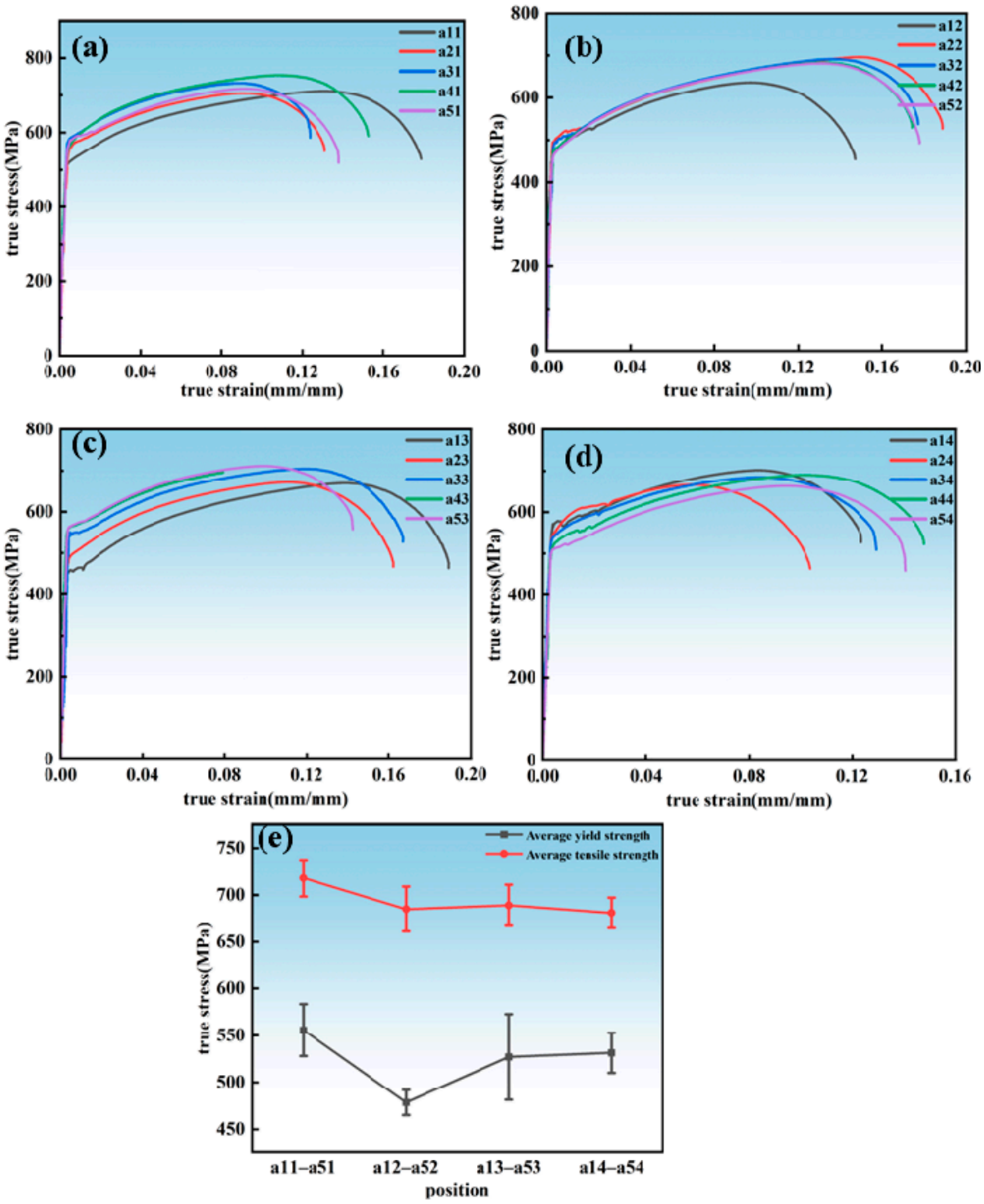


Figure 6. Uniaxial tensile true stress–strain curves of the materials in cap weld: (**a**) a11–a51; (**b**) a12–a52; (**c**) a13–a53; (**d**) a14–a54; (**e**) the average performance at each of the four positions.

Four specimens were tested in the direction of the wall thickness along the lower filling weld. The yield strength ranged from 544 to 646 MPa, while the tensile strength varied from 687 to 781 MPa. The closer the test was to the bottom, the greater the yield strength observed.

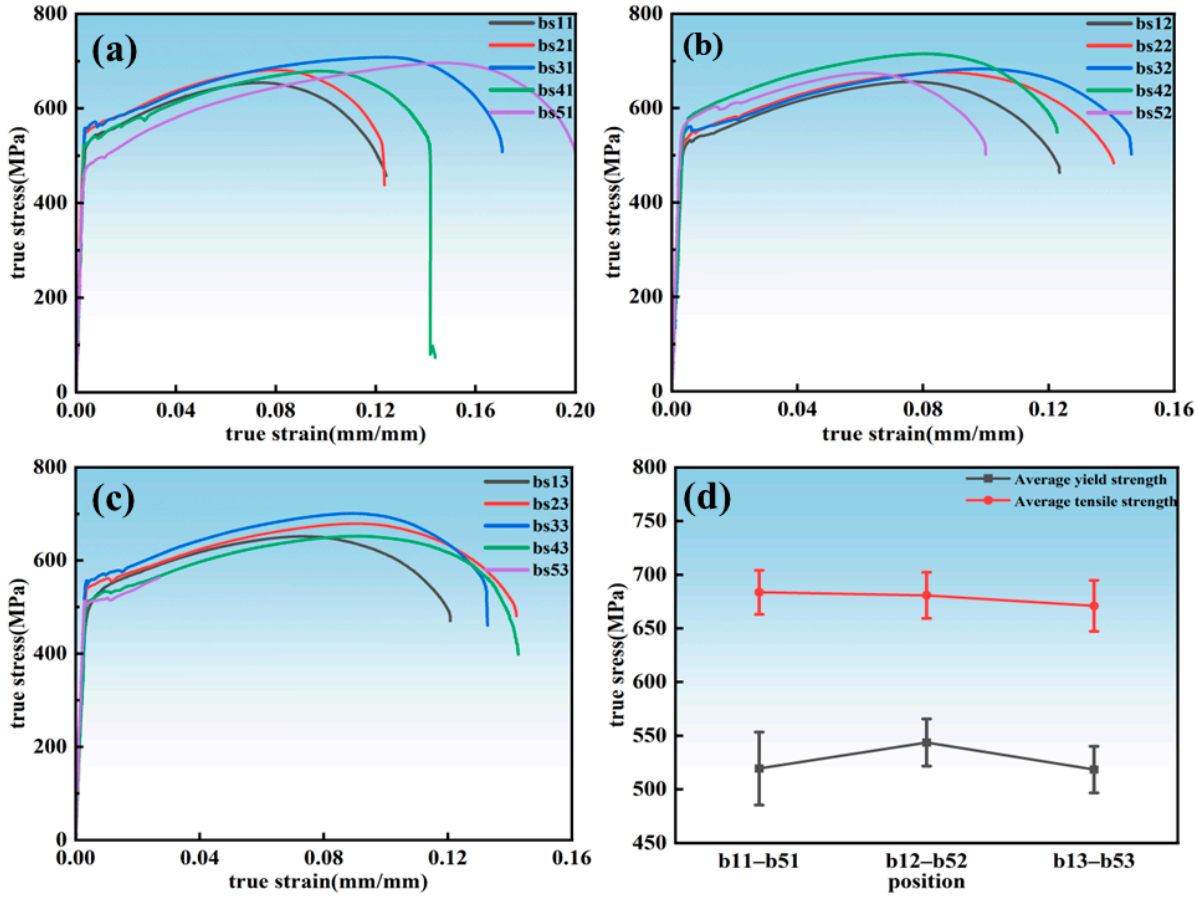


Figure 7. Uniaxial tensile true stress–strain curves of the materials in upper filling weld: (**a**) bs11–bs51; (**b**) bs12–bs52; (**c**) bs13–bs53; (**d**) the average performance at each of the three positions.

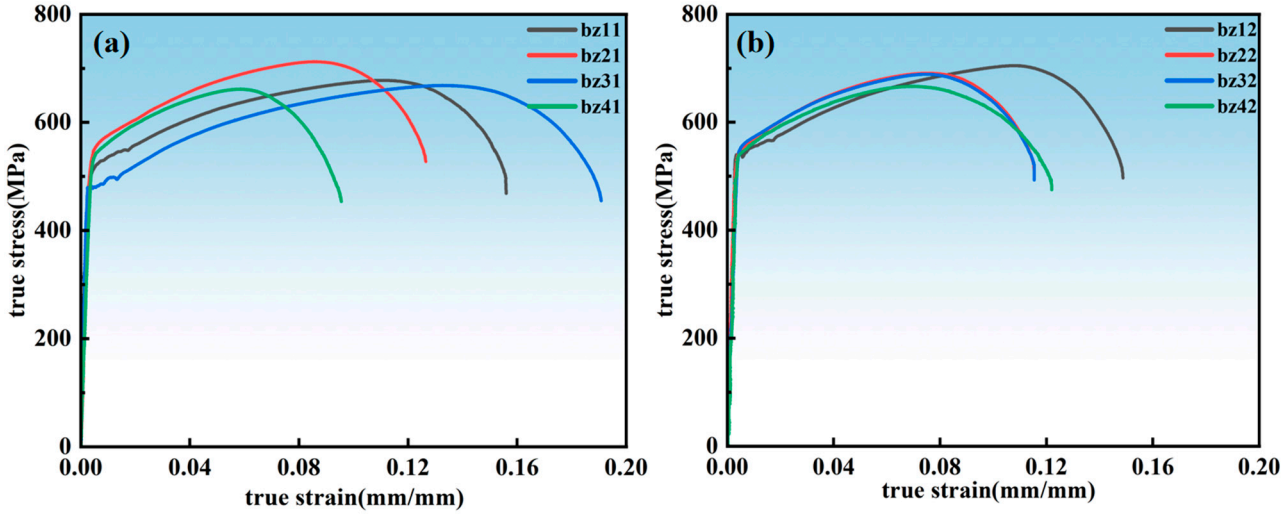


Figure 8. Uniaxial tensile true stress–strain curves of the materials in middle filling weld: (**a**) bz11–bz51; (**b**) bz12–bz52.

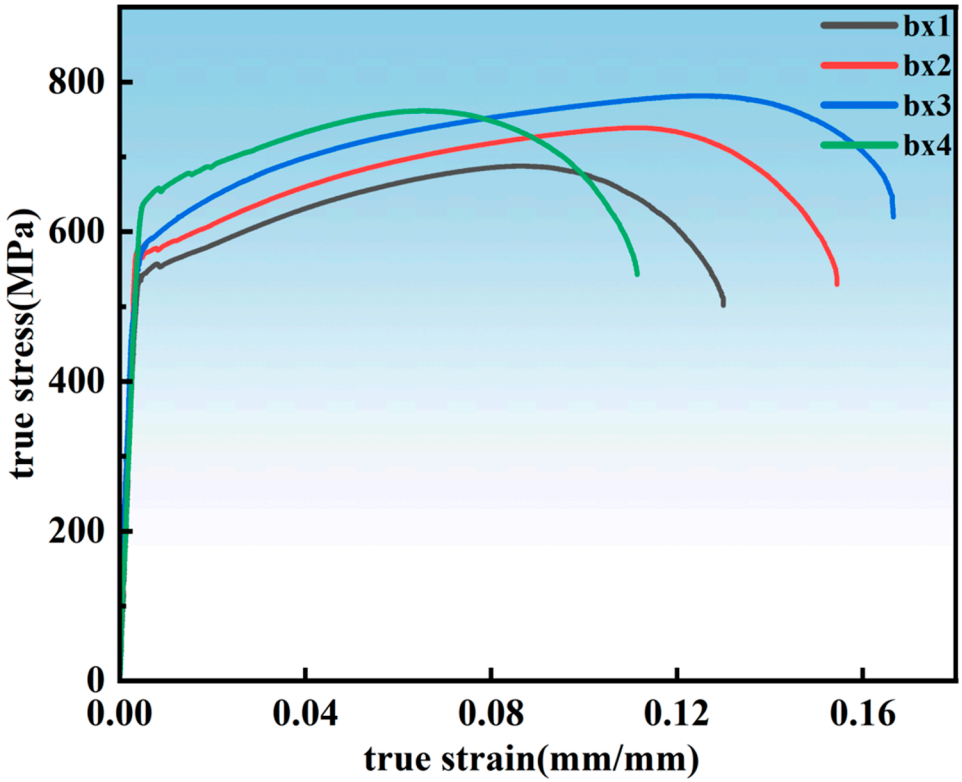


Figure 9. Uniaxial tensile true stress–strain curves of the materials in lower filling weld.

Figure 10 presents the uniaxial tensile test results of root bead zone specimens. The two specimens exhibit significant dispersion, but the yield strength of specimen c1 reaches as high as 570 MPa.

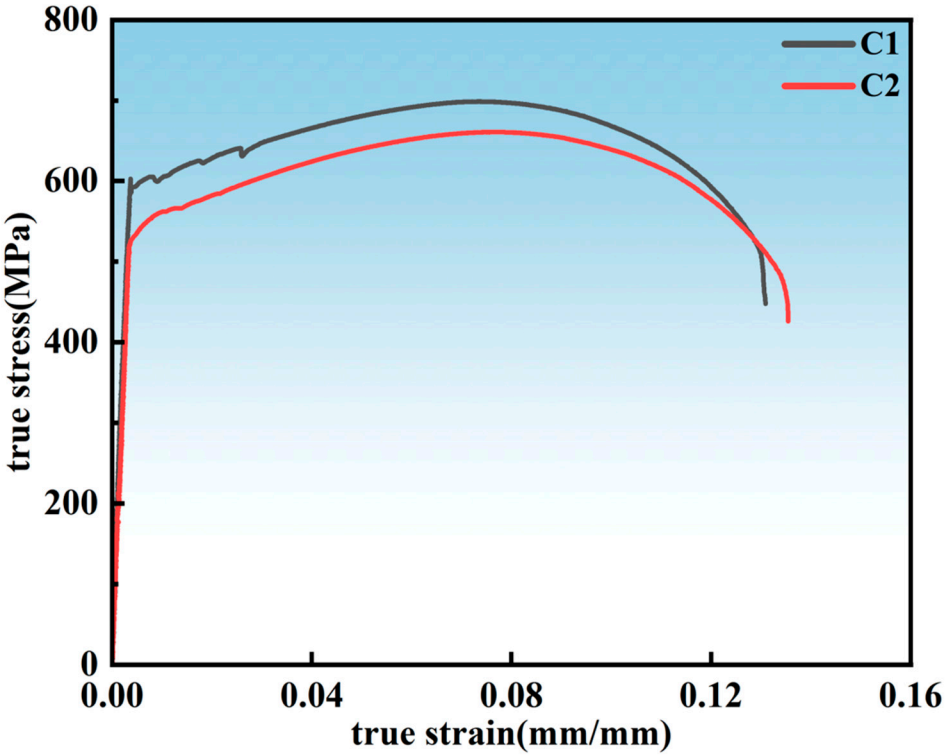


Figure 10. Uniaxial tensile true stress–strain curves of the materials in root bead.

3.2. Heat-Affected Zone

The uniaxial tensile test results of specimens from the heat-affected zone are shown in Figure 11a,b. The true stress–strain curves for the four specimens on the left side (X80 steel side, specimens d1–d4) are illustrated in Figure 11a, demonstrating a significant degree of scatter, with yield strengths ranging from 500 to 600 MPa. Similarly, the curves for the four specimens on the right side (X60 steel side, specimens ne1–ne4) are presented in Figure 11b, also exhibiting considerable scatter, with yield strengths between 450 and 550 MPa. It can be observed that the strength of the heat-affected zone on the left side is higher than that on the right side, which is consistent with the fact that the strength of the base material on the left side (X80) is greater than that on the right side (X60). In the direction of wall thickness, the strength of the cap weld and the root bead is higher than that of the filling weld.

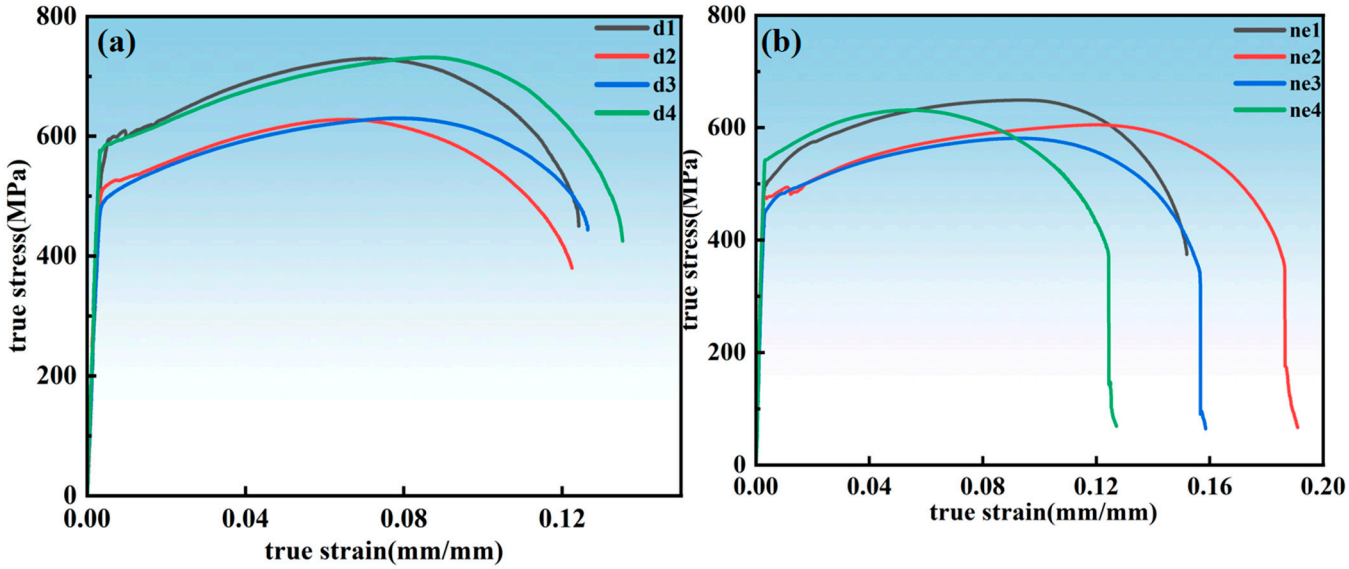


Figure 11. Uniaxial tensile true stress–strain curves of the materials in heat-affected zone: (**a**) d1–d4; (**b**) ne1–ne4.

3.3. Base Metal

The results of the uniaxial tensile tests conducted on base metal zone specimens are presented in Figure 12a–f. Notably, specimens X80z1, X60s4, and X60x1 experienced failure during testing, resulting in the absence of valid data. As illustrated in Figure 12a, the true stress–strain curves of the five specimens exhibit a certain degree of dispersion, whereas the test results from specimens in other zones demonstrate good repeatability. The overall yield strength for the X80 base metal ranged from 456 to 547 MPa, while the yield strength for the X60 base metal varied from 464 to 522 MPa.

3.4. Mechanical Property Differences in the Thickness Direction of Welds

Comparing the average yield strength and tensile strength in the direction of the weld seam center wall thickness. Figure 13 illustrates the average tensile properties of the weld seam across five regions along the wall thickness direction (cap weld–upper layer of the fill weld–middle layer–lower layer–root bead). The mechanical properties of the weld zone show significant variation along the thickness direction, with the lowest average yield strength at 533 MPa and the highest at 570 MPa.

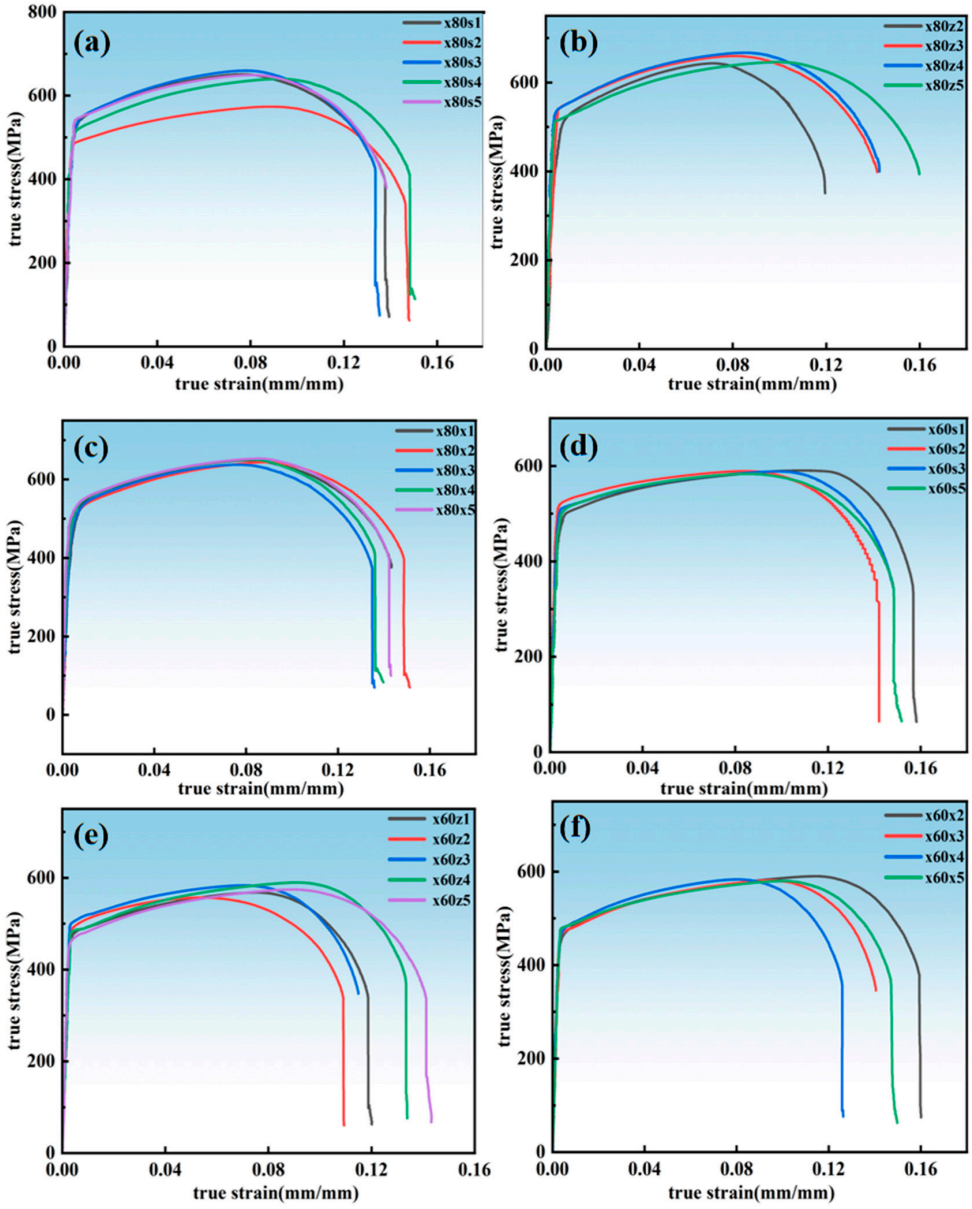


Figure 12. Uniaxial tensile true stress–strain curves of the base metal: (**a**) X80s1–s5; (**b**) X80z1–z5; (**c**) X80x1–x5; (**d**) X60s1–s5; (**e**) X60z1–z5; (**f**) X60x1–x5.

The tensile performance of the root bead is the highest, followed by the fill weld, while the cap weld exhibits the lowest performance. The differences in strength properties are a result of the coupling and superposition of welding thermal effects and welding processes. The cross-section of the weld seam is V-shaped, with the root bead being the first operation in the welding process. The width of the root bead is the narrowest among all welds, resulting in the heat generated during welding being transferred to the BM at a faster rate. The rapid cooling often leads to the formation of hardened microstructures, resulting in high hardness and poor toughness.

In filling welds, the width of the weld bead is wider compared to that of the root weld. As one moves closer to the cap weld, the width of the weld bead increases. The heat generated during welding is less likely to dissipate through the base material, resulting in a slower cooling rate, which reduces the tendency for hardening. With subsequent weld beads reheating the previous layers, grain refinement and tempering of the hardened

structure are achieved. The results indicate that the yield strength of specimens closer to the cap weld is lower.

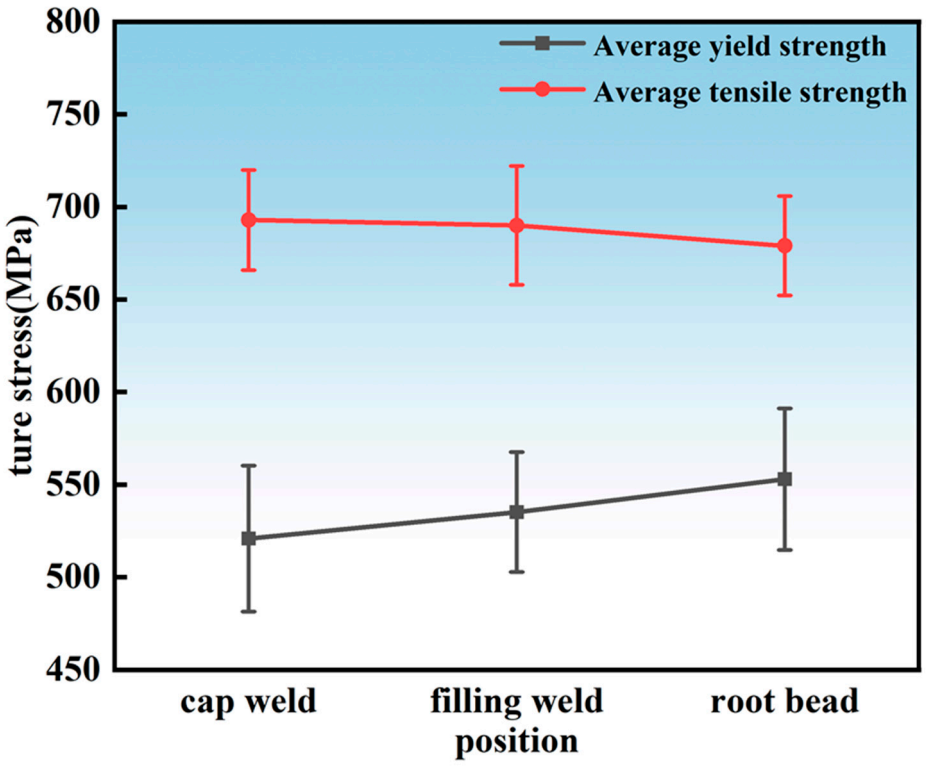


Figure 13. Average tensile properties in different regions along the weld thickness direction.

The weld bead of the capping layer is the widest. However, it cools slowly as it can only transfer heat to the air, and it is not tempered by subsequent passes. As a result, its grains are often relatively coarse, and its structural compactness is lower than that of the filling layer; nonetheless, this is also influenced by the welding materials and processes. Unlike filled and root welds, it is not possible to determine whether the welding process or heat conduction during welding is the main factor leading to this outcome.

3.5. Mechanical Property Differences in Transverse Welds

The average tensile properties across the five major regions along the weld seam (X80 base metal zone, heat-affected zone (d), weld zone, heat-affected zone (ne), and X60 base metal zone) are illustrated in Figure 14. It is evident that the average yield strength of the X80 base metal zone is 522 MPa, with a tensile strength limit of 645 MPa, which is significantly higher than the average yield strength of 484 MPa and tensile strength limit of 581 MPa in the X60 base metal zone. This discrepancy is likely related to the inherent material differences between the two base metal zones. The average yield strength of the heat-affected zone (d) is 541 MPa, with a tensile strength limit of 680 MPa, which is also notably higher than the average yield strength of 490 MPa and tensile strength limit of 617 MPa in the heat-affected zone ne. This difference is closely associated with the proximity of the heat-affected zone (d) to the high-strength X80 base metal zone, while the heat-affected zone ne is near the relatively lower-strength X60 base metal zone.

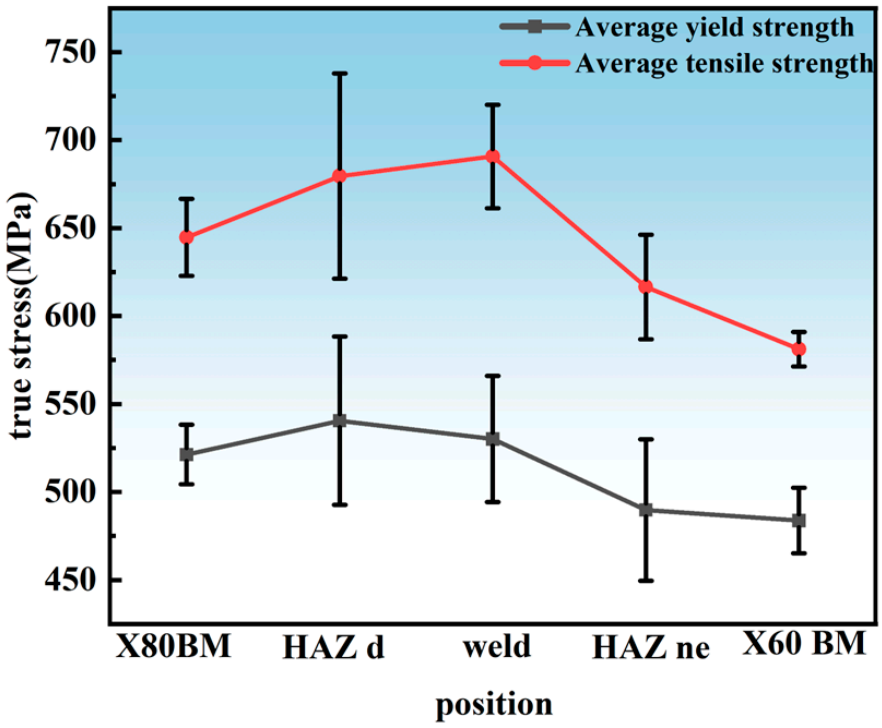


Figure 14. Average tensile properties of different zones along the transverse direction of the weld.

In Figure 14, the maximum HAZ is observed on the X80 side. One reason for this is the greater thickness of the base material on the X80 side, which leads to a faster cooling rate, making it more susceptible to the formation of hardened microstructures compared to the X60 side. Additionally, the X80 side exhibits higher strength, with the microstructure in its HAZ primarily consisting of higher-strength structures such as polygonal ferrite, martensite, retained austenite, and granular bainite, and contains almost no ferrite.

Table 1 shows that the base metal of X80 steel contains 1.68% Mn and 0.21% Ni, the base metal of X60 steel contains 1.36% Mn and 0.011% Ni, and the girth weld metal contains 1.69% Mn and 0.21% Ni. The girth weld metal exhibits the highest manganese content, while its nickel content is equal to that of the X80 steel base metal and higher than that of the X60 steel base metal. Manganese and nickel are substitutional solid solution elements in austenite and ferrite. The atomic radii of these elements differ significantly from that of iron, leading to lattice distortion that hinders dislocation movement and thereby provides considerable solid solution strengthening [29,30]. Consequently, increasing the concentrations of manganese and nickel enhances the strength of the weld metal. Avazkonandeh et al. found that higher nickel and manganese contents in the weld metal of high-strength pipeline steel significantly increased both the strength and the proportion of acicular ferrite [31–33]. Therefore, the observed order of tensile strength is as follows: the girth weld metal is the highest, followed by the X80 steel base metal, and the X60 steel base metal is the lowest.

4. Conclusions

Overall, this study demonstrates that heterogeneous girth welds in unequal wall thickness X80/X60 pipelines exhibit pronounced mechanical property gradients, and that such non-uniformity must be explicitly considered in structural integrity and safety evaluations. On this basis, the main conclusions are:

(1) A micro-tensile specimen methodology was established for heterogeneous girth welds with non-uniform wall thicknesses. The weld cross-section was subdivided into several characteristic zones according to metallographic features, and specimens were

carefully designed and machined following the natural morphology of each zone. This approach enables accurate determination of local tensile properties within the X80/X60 girth weld.

(2) The test results reveal marked differences in mechanical properties among the various characteristic zones, with clear gradients both through the wall thickness and in the transverse direction. These findings confirm that the girth weld cannot be regarded as a quasi-homogeneous material.

(3) The observed non-uniformity in material properties is mainly attributed to the combined effects of different welding consumables, wall thickness mismatch between X80 and X60 pipes, and variations in heat dissipation and cooling rates during welding, which together lead to distinct microstructures and property distributions.

(4) The results highlight the limitations of traditional evaluation methods that either homogenize the weld region or simply substitute BM properties for those of the girth weld. For heterogeneous non-uniform wall thickness joints, the spatial variation in material properties must be explicitly incorporated into weld safety evaluations and integrity assessment procedures.

It is important to note that while the micro-tensile testing method employed in this study is universally applicable for characterizing mechanical property gradients in welded joints, the specific findings obtained—such as the location and extent of the softened zone, as well as the magnitude of property transitions across different regions—are primarily characteristic of the particular material combination (X80/X60), the corresponding strength mismatch level, the specific welding procedure adopted, and the given wall thickness ratio. The principal advantage of this method lies in its ability to accurately reveal the unique distribution characteristics of properties in such complex joints. However, extrapolating the quantitative results of this study to other material systems or geometric configurations should be approached with caution and validated through further experimentation.

Author Contributions: Conceptualization, K.W.; methodology, K.W. and W.M.; software, J.R.; validation, M.Z.; formal analysis, J.L. and J.R.; investigation, J.C. and C.T.; resources, M.Z., J.C. and C.T.; data curation, C.T. and K.W.; writing—original draft preparation, K.W.; writing—review and editing, K.W. and M.Z.; visualization, H.N. and J.L.; supervision, C.T. and H.N.; project administration, M.Z. and W.M.; funding acquisition, M.Z. All authors have read and agreed to the published version of the manuscript.

Funding: This work was supported by National Key R&D Program of China (No. 2023YFB4606604) and CNPC Science and Technology Project (No. 2023ZZ11-04).

Data Availability Statement: The original contributions presented in this study are included in the article. Further inquiries can be directed to the corresponding author.

Conflicts of Interest: Authors Ke Wang, Weifeng Ma, Hailiang Nie and Junjie Ren were employed by the company Tubular Goods Research Institute, China National Petroleum Corporation (CNPC). Author Junfeng Cao was employed by the Production and Operation Department of Changqing Oilfield Company. Author Chaocheng Tan was employed by The Tenth Oil Production Plant of Changqing Oilfield Company. The remaining authors declare that the research was conducted in the absence of any commercial or financial relationships that could be construed as a potential conflict of interest. The authors declare that this study received funding from CNPC. The funder was not involved in the study design, collection, analysis, interpretation of data, the writing of this article or the decision to submit it for publication.

References

1. Zhang, Z.L.; Hauge, M.; Thaulow, C.; Ødegård, J. A notched cross weld tensile testing method for determining true stress–strain curves for weldments. *Eng. Fract. Mech.* **2002**, *69*, 353–366. [CrossRef]
2. Zhang, T.; Shuai, Y.; Shuai, J.; Lv, Z.; Zhang, J.; Zhang, Y.; Wang, X.; Zhang, L. Study on fracture behaviour of pipeline girth welds based on curved wide plate specimens: Experimental and numerical analysis. *Eng. Fract. Mech.* **2024**, *311*, 110522. [CrossRef]
3. Zhang, Y.; Shuai, J.; Lv, Z.; Zhang, T. Study on fracture behavior of pipeline girth weld based on CTOD-Am method and Gurson ductile damage model. *Theor. Appl. Fract. Mech.* **2023**, *123*, 103692. [CrossRef]
4. Zhang, Y.; Shuai, J.; Ren, W.; Lv, Z. Investigation of the tensile strain response of the girth weld of high-strength steel pipeline. *J. Constr. Steel Res.* **2022**, *188*, 107047. [CrossRef]
5. Hertelé, S.; O'Dowd, N.; Van Minnebruggen, K.; Denys, R.; De Waele, W. Effects of pipe steel heterogeneity on the tensile strain capacity of a flawed pipeline girth weld. *Eng. Fract. Mech.* **2014**, *115*, 172–189. [CrossRef]
6. Zhang, D.; Liu, X.; Kong, T.; Yang, Y.; Fu, M.; Wang, H.; Wu, K.; Zhang, H. A novel method for determining the stress-strain constitutive relationship of high-grade pipeline weld zone material. *Eng. Fail. Anal.* **2023**, *150*, 107318. [CrossRef]
7. Kong, L.; Shuai, J.; Zhou, X.; Chao, Y.; Han, K. A universal method for acquiring the constitutive behaviors of API-5 L X90 welds. *Exp. Mech.* **2016**, *56*, 165–176. [CrossRef]
8. Tu, S.; Ren, X.; He, J.; Zhang, Z. A method for determining material's equivalent stress-strain curve with any axisymmetric notched tensile specimens without Bridgman correction. *Int. J. Mech. Sci.* **2018**, *135*, 656–667. [CrossRef]
9. Hertelé, S.; Van Minnebruggen, K.; Verstraete, M.; Denys, R.; De Waele, W. Influence of pipe steel heterogeneity of the upper bound tensile strain capacity of pipeline girth welds: A validation study. *Eng. Fract. Mech.* **2016**, *162*, 121–135. [CrossRef]
10. Tu, S.; Ren, X.; He, J.; Zhang, Z. Stress–strain curves of metallic materials and post-necking strain hardening characterization: A review. *Fatigue Fract. Eng. Mater. Struct.* **2020**, *43*, 3–19. [CrossRef]
11. Zhang, S.; Cheng, Y.; Wang, R.; Feng, X.; Feng, Q.; Wei, L.; Wang, R.J.; Duo, Y.Q.; Han, Y. Performance characteristics and technical challenges of X80 pipeline steel. *Oil Gas Storage Transp.* **2019**, *38*, 481–495.
12. Hertelé, S.; O'Dowd, N.; Van Minnebruggen, K.; Verstraete, M.; De Waele, W. Fracture mechanics analysis of heterogeneous welds: Numerical case studies involving experimental heterogeneity patterns. *Eng. Fail. Anal.* **2015**, *58*, 336–350. [CrossRef]
13. Cao, Y.; Zu, Y.; Zhen, Y.; Li, F.; Wu, G. Determination of the true stress-strain relations of high-grade pipeline steels based on small punch test correlation method. *Int. J. Press. Vessel. Pip.* **2022**, *199*, 104739. [CrossRef]
14. Zu, Y.; Cao, Y.; Zhen, Y.; Li, F.; Wu, G. Determination on the fracture toughness of the welded joints of X80 pipeline steels based on small punch test. *Eng. Fract. Mech.* **2023**, *291*, 109525. [CrossRef]
15. Zuniga, S.M.; Sheppard, S.D. Determining the constitutive properties of the heat-affected zone in a resistance spot weld. *Model. Simul. Mater. Sci. Eng.* **1995**, *3*, 391. [CrossRef]
16. Wei, C.; Zhang, J.; Yang, S.; Tao, W.; Wu, F.; Xia, W. Experiment-based regional characterization of HAZ mechanical properties for laser welding. *Int. J. Adv. Manuf. Technol.* **2015**, *78*, 1629–1640. [CrossRef]
17. Zhan, M.; Du, H.; Liu, J.; Ren, N.; Yang, H.; Jiang, H.; Diao, K.; Chen, X. A method for establishing the plastic constitutive relationship of the weld bead and heat-affected zone of welded tubes based on the rule of mixtures and a microhardness test. *Mater. Sci. Eng. A* **2010**, *527*, 2864–2874. [CrossRef]
18. Pham, T.H.; Kim, S.E. Determination of mechanical properties in SM490 steel weld zone using nanoindentation and FE analysis. *J. Constr. Steel Res.* **2015**, *114*, 314–324. [CrossRef]
19. Adeeb, S.; Horsley, D.; Yan, J.; Sutton, M.A.; Reynolds, A.P. Local stress-strain response of an axial X100 girth weld under tensile loading using digital image correlation. In *The International Pipeline Conference*; ASME: New York, NY, USA, 2006.
20. Wu, X.; Shuai, J.; Xu, K.; Lv, Z.; Shan, K. Determination of local true stress-strain response of X80 and Q235 girth-welded joints based on digital image correlation and numerical simulation. *Int. J. Press. Vessel. Pip.* **2020**, *188*, 104232. [CrossRef]
21. Cao, J.; Ma, W.; Hui, W.; Wang, K.; Cai, K.; Li, X.; Cong, S.; Ren, J.; Nie, H.; Dang, W. Effects of strain path and girth weld heterogeneity on strain limits of X70 pipeline. *Int. J. Press. Vessel. Pip.* **2022**, *198*, 104682. [CrossRef]
22. Sharma, S.K.; Maheshwari, S. A review on welding of high strength oil and gas pipeline steels. *J. Nat. Gas Sci. Eng.* **2017**, *38*, 203–217. [CrossRef]
23. Tang, Z.B.; Xu, F.; Xu, Z.J.; Li, Y.L.; Li, P.Z. Research onmechanical properties of micro-zones of welding line. *J. Mech. Strength* **2010**, *32*, 58–63. (In Chinese)
24. Zhu, M.H. Study of Test Methods of Mechanical Properties of Microspecimen Material Under High-Temperature Environment. Master's Thesis, NorthwesternPolytechnical University, Xi'an, China, 2006. (In Chinese)
25. Nie, H.; Ma, W.; Xue, K.; Ren, J.; Dang, W.; Wang, K.; Cao, J.; Yao, T.; Liang, X. A novel test method for mechanical properties of characteristic zones of girth welds. *Int. J. Press. Vessel. Pip.* **2021**, *194*, 104533. [CrossRef]
26. *Q/SY GJX0221-2012*; Technical Specification for Welding of Station Pipeline Networks in the West–East Gas Pipeline Phase III Project. China Petroleum Publishing House: Beijing, China, 2012.

27. *GB/T8110-2008*; Welding Electrodes and Rods for Gas Shielding Arc Welding of Carbon and Low Alloy Steel. Standard Press of China: Beijing, China, 2009.
28. *GB/T5118-2012*; Covered Electrodes for Manual Metal Arc Welding of Creep-Resisting Steels. Standard Press of China: Beijing, China, 2012.
29. Han, S.Y.; Shin, S.Y.; Seo, C.-H.; Lee, H.; Bae, J.-H.; Kim, K.; Lee, S.; Kim, N.J. Effects of Mo, Cr, and V additions on tensile and Charpy impact properties of API X80 pipeline steels. *Metall. Mater. Trans. A* **2009**, *40*, 1851–1862. [CrossRef]
30. Mohrbacher, H.; Kern, A. Nickel alloying in carbon steel: Fundamentals and applications. *Alloys* **2023**, *2*, 1–28. [CrossRef]
31. Sheykh Jaberi, F.; Kokabi, A.H. Influence of Nickel and Manganese on Microstructure and Mechanical Properties of Shielded Metal Arc-Welded API-X80 Steel. *J. Mater. Eng. Perform.* **2012**, *21*, 1447–1454. [CrossRef]
32. Zhang, Y.; Qi, L.; Song, P.; Wang, Y.; Chen, Y.; Zhou, Y. Effect of Mo and Ni on Properties and Weldability of X70 Line Pipe. *Pet. Pet. Tubul. Goods Instrum.* **2022**, *8*, 21–25. (In Chinese)
33. Guo, B.; Deng, C.; Gong, B.; Liu, Y.; Ning, J.; Zhang, K. Numerical Investigation of the Influence of Geometric Features and Weld Metal Properties on Stress and Strain States in X80 Girth Welds. *Metals* **2025**, *15*, 986. [CrossRef]

Disclaimer/Publisher's Note: The statements, opinions and data contained in all publications are solely those of the individual author(s) and contributor(s) and not of MDPI and/or the editor(s). MDPI and/or the editor(s) disclaim responsibility for any injury to people or property resulting from any ideas, methods, instructions or products referred to in the content.